DOI: 10.13009/EUCASS2022-7219
9TH EUROPEAN CONFERENCE FOR AERONAUTICS AND SPACE SCIENCES (EUCASS)

Preliminary Design of a Space Vehicle for Active Debris Removal (ADR): PERSEPHONE

Elise Meisse, Juan Esteban Martinez-Morales***
IPSA Institut Polytechnique des Sciences Avancées
63 Bis Boulevard de Brandebourg, 94200 Ivry-sur-Seine, France
**meisseelise@gmail.com*
***steb.aero@gmail.com*

Abstract

Space sustainability is being threatened by the proliferation of space debris, especially in low Earth orbits (LEO). PERSEPHONE (Performing Space Environment Protection from Hazardous Objects by Net Elimination) is a small spacecraft concept for active debris removal, devoted to removing large-sized debris in LEO. A new approach is the use of a debris-capture net whose rope is used as electrodynamic tether (EDT) for a passive descent phase, combined with multimode chemical propulsion for impulsive maneuvers, station keeping, and a final boost that leads to controlled atmospheric re-entry. The current work is the first to consider such a propulsive configuration for an ADR mission.

1. Introduction

By May 2022, there were orbiting the Earth around 130 million of debris from 1mm to 1 cm, 1 million objects from 1 cm to 10 cm, and 36500 objects greater than 10 cm [1] including dead satellites and rocket bodies. The company LeoLabs reported in 2020 that the possible potential collision scenarios (known as conjunctions) in a single day are about 800000 [2] and that most of these high-risk events involve space debris. The space operations in orbit are being more and more compromised by space debris. This number will continue increasing due to two main drivers: the proliferation of space debris crashing and creating more debris, plus the increase in space traffic.

When a collision occurs, a junk cloud is generated and spread in all directions. The debris of this cloud can hit other debris or satellites, which results in other clouds that repeat the cycle. This phenomenon is known as Kessler syndrome, which unfortunately already started in LEO. This region contains most of the population of space debris, and the biggest clusters are between 700 and 1000 km altitude [3] where most of the break-ups and collisions have occurred.

On the other hand, the orbital traffic increased dramatically in the last years [4]. Just in the 2 last years, the number of operational satellites doubled up [5] to approximately 5800 [1], and it is expected to increase to 150000 in the next decade [5], which is 25 times more.

PERSEPHONE spacecraft is a solution that aims to address this issue by active debris removal of the most massive debris in LEO. These large debris release thousands of new fragments when there is a collision, representing a major risk to operational satellites. This paper presents a selection of the studies performed during the preliminary design, with a special focus on the mission design, electrodynamic tether, propulsion subsystem, and capture subsystem.

2. Mission design

This section presents an overview of the high-level requirements that led the mission design with a space sustainability approach. It also discusses the features of the space debris target selection, and a brief explanation of the mission profile phases with methods and results from the analysis performed for each of them.

2.1 Mission requirements

PERSEPHONE's mission is engaged with space sustainability, thus the high-level mission requirements comply with the Inter Agency Space Debris Coordination Committee (IADC) guidelines [6] and the ISO standard requirements [7], particularly the following points.

1) Limitation of debris released during normal operations: no debris is released during any phase of the mission and both the vehicle and the target are disposed by performing a controlled re-entry.

DOI: 10.13009/EUCASS2022-7219

2) Minimization of the potential for on-orbit break-ups: the vehicle has an agile maneuver capability in the 6 degrees of freedom (DOF), and the capture mechanism selected does not bring a risk of component break-ups during the target's capture.
3) Post-mission disposal (limitation of the on-orbit lifetime): the mission has a duration of less than one year and the vehicle can de-orbit itself (even within the frame of 25 years [6] [7] in case of mission failure).
4) Post-mission disposal (limitation of casualties on-ground due to uncontrolled re-entries): the casualty risk probability is lower than 1×10^{-4} [6].
5) Prevention of on-orbit collisions: the risk of the EDT being hit by debris of different sizes along the mission duration was analyzed, and the probabilities are within acceptable values. The EDT system can be turned on/off for collision avoidance maneuvers.

2.2 Target selection

PERSEPHONE's demonstration mission considers European debris due to current political limitations. It is found that among the 50 top debris that must be removed first [4], two satisfy this criterion: the ENVISAT and one Ariane 5 upper stage. The last one, with NORAD 27387, was selected and used throughout the different analyses of this study. Its launch corresponds to Vol. 145 on March 1st, 2002, with an Ariane 5-G [8] whose payload was the ENVISAT (Figure 1 left). This remark is elemental because there is a significant difference: Ariane-5G uses an EPS (Storable Propellant Stage, bipropellant propulsion) for the upper stage, while the Ariane 5-ECA uses the ESC-A (Cryogenic Upper Stage Type A), changing the components, dimensions and total mass. The corresponding configuration (see Figure 1) is composed by the EPS, a Launch Vehicle Adaptor (LVA) 3936, a Vehicle Equipment Bay (VEB), and a Payload Adapter System (PAS) 2624 [9]. It has a total mass of 2575 kg (considering remnants of propellant), and it is orbiting at an altitude between 796 and 748 km with an inclination of 98.7° [10].

Figure 1 : Space debris NORAD 27387 Ariane 5-G upper stage with the payload (ENVISAT) integrated above before the launch (left), and the components corresponding to its configuration.

2.3 Mission profile and analysis

The mission profile is illustrated by the Figure 2, and detailed within the next paragraphs.

Launch: It was assumed for the demonstration mission a launch from the CSG (Guiana Space Centre) in Kourou. The demonstration mission analysis considered two possible types of launch.

Dedicated launch: PERSEPHONE would be the main passenger. This allows to determine the orbital conditions of the injection but would require paying most of the launch cost, or the total if it is the only passenger.

Piggyback launch: PERSEPHONE would be placed in the free space not being used by the main passenger, importantly reducing costs but losing the right to determine the conditions of the injection's orbit. The piggyback launch demands higher performance for the spacecraft and sizing it with these conditions provide PERSEPHONE the capability of taking any of the two types of launch.

DOI: 10.13009/EUCASS2022-7219

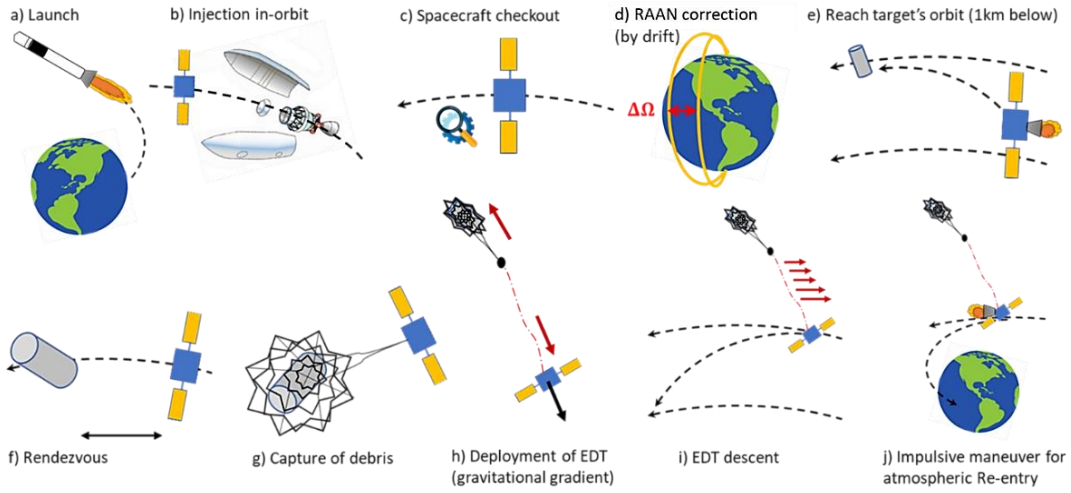

Figure 2: Mission profile of PERSEPHONE.

Injection: The orbit of the target has an eccentricity of 0.00335, with a maximum altitude difference of 48 km between apogee and perigee. Hence, it was assumed a circular orbit throughout the different phases to simplify the analysis of the trajectory, taking the altitude of the apogee (796 km) as a semimajor axis. Consequently, the injection orbit was also assumed as circular.

Dedicated launch, the spacecraft would be injected in an orbit with an altitude of 795 km (1 km under the target's orbit for safety) ± 15 km (injection's accuracy), an inclination of 98.67° (target) ± 0.15° (injection's accuracy), and RAAN of 17.56° (target) ± 0.2° (injection's accuracy).

Piggyback launch: it was assumed the use of the VEGA launcher for analytical purposes. This is a European launcher that offers piggyback launches and is typically used for missions in LEO. Most of its orbital injections are in SSO (sun-synchronous orbit), a region that in fact contains clusters of the most concerning debris [4]. The values of the injection's accuracy are taken from the Vega User's Manual [11]: ± 0.15° for inclination and ± 0.2° for RAAN. Therefore, the injection orbit can have an altitude between 600 - 800 km (SSO) ± 15 km (injection's accuracy), an inclination of 98° - 99°(SSO) ± 0.15° (injection's accuracy), and a RAAN of 17.56° (target) ± 0.2° (injection's accuracy) ± 3.5° (defined during next phase).

RAAN correction and reaching the target's orbit: the RAAN value at the injection might need to be corrected due to the accuracy of the launcher, therefore the spacecraft would need to change its altitude using a Hohmann transfer maneuver, then it waits until the RAAN is corrected by the effect of drift at different altitudes due to J2 perturbation, and finally it performs another Hohmann transfer maneuver to reach an orbit 1 km under the target. The last maneuver also circularizes the orbit and corrects the inclination's difference caused by the injection's accuracy. After estimating the time for the rest of the phases (~ 246 days) and considering the mission's total time requirement inferior to 365 days, it was proposed a maximum margin of 100 days for this phase.

Dedicated launch: in the scenario with the less-optimal RAAN injection's accuracy (± 0.2°) it would take 413 days to correct by drift it stays in the injection's orbit, which exceeds the required time of the mission. In such a scenario, PERSEPHONE would be able to correct the RAAN in 91.5 days by just changing the altitude to ±4 km.

Piggyback launch: the injection's altitude specified by the main passenger could be convenient in the case where the RAAN difference is corrected by drift without moving from orbit, but the Δv cost to switch to the altitude 1 km under the target is higher than for a dedicated launch. After some trade-offs between Δv cost and time duration for the phase, it was defined a margin of ± 3.5° RAAN (additional to the injection's accuracy ± 0.2°) for compatible piggyback launches with the PERSEPHONE's mission. In such cases, the spacecraft can move ± 75 km altitude to correct the RAAN in a maximum of 100 days.

Rendezvous (phasing): After reaching the altitude of 1 km just below the target's orbit (for safety), PERSEPHONE will be either ahead or behind the target, and must approach the debris to a separation of just 10 km using a phasing maneuver. To compute this separation, it was considered the drift created by different angular velocities between the orbit of RAAN correction and the orbit 1km below target. It was assumed that the drift of one orbital period was a valid approximation to estimate the distance between the target and spacecraft in the less optimal scenario. To calculate this, it was used the equation $\Delta L = 3\pi\Delta z$ suggested in [12], where ΔL is the drift per orbit and Δz is the altitude difference. It was found that the separation ahead or behind the target would be 1319.47 km maximum when arriving

DOI: 10.13009/EUCASS2022-7219

the orbit of 1km below, if PERSEPHONE is launched in piggyback and injected at an altitude of 600 km (SSO) minus 15 km (injection's accuracy).

Rendezvous (approach): In the local reference frame of the target, it is needed to distinguish two directions called R-bar and V-bar which are respectively the axis in direction of the orbital movement and the axis that points towards the center of the Earth. A hopping maneuver in either V-bar or R-bar (see Figure 3) has safety and operational advantages. Every hop requires two boosts, serving the second one to stop the motion at the desired point and begin the consecutive hop. If the second boost is not performed for any control failure and there are no disturbances, the chaser will naturally return to its previous point symmetrically allowing the chance to recover the mission.

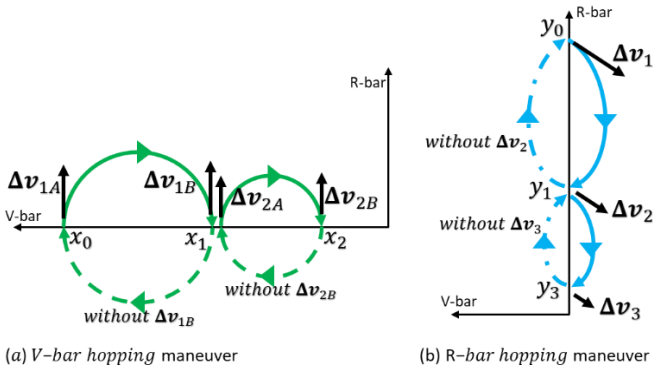

(a) *V–bar hopping* maneuver (b) R–*bar hopping* maneuver

Figure 3: Schematics and passive safety of V-bar and R-bar approaches.

Being 1 km under the target's orbit, PERSEPHONE's approach strategy consists of a first hopping maneuver in V-bar from 10 km to 0 m, followed by another hopping maneuver in R-bar from 1 km to 15 m distance below the target, as shown in Figure 4. This strategy offers a layout that is appropriate for the deployment of the EDT after the capture, which needs to be released in a radial direction to generate the Lorentz force.

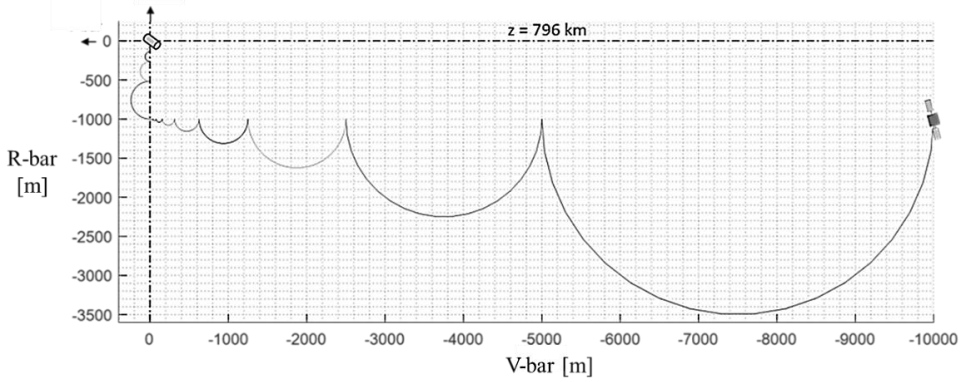

Figure 4: PERSEPHONE's R-bar rendezvous approach strategy.

For the computation of the hops in V-bar, it was used the method suggested in [12], where $\Delta v_1 = \Delta v_2 = (n/4)\Delta x$, where Δv_1 and Δv_2 correspond to the propulsive boost at the beginning and the end of each hop, n is the angular velocity of the reference orbit (796 km) and Δx is the length of each hop. This equation was implemented in an iterative computation with MATLAB, where every hop approaches the half of the distance left between the spacecraft and the target. For the R-bar hopping maneuver, the computations were based on the method of Changxuan and Pini [13] and implemented in an iterative MATLAB code. The total Δv required for the whole rendezvous phase is shown in the Equation 1.

$$\Delta v_{Rendezvous} = \Delta v_{Phasing} + \Delta v_{V-bar} + \Delta v_{R-bar} = 22.8\frac{m}{s} + 5.19\frac{m}{s} + 4.14\frac{m}{s} \quad (1)$$

Station keeping for capture: Once 15 m under the target, the spacecraft must keep its position (Figure 5a) until the monitoring and capture are completed. For this, the spacecraft must perform a continuous thrust maneuver, to move in a straight line along V-bar. For the calculation of Δv cost, Fehse [12] suggests the equation: $\Delta v = -3\omega^2 Z_0 \Delta t$, where ω is the angular velocity of the target, Z_0 is the difference of altitudes and Δt is the time of the maneuver. Therefore, for

DOI: 10.13009/EUCASS2022-7219

every orbital period (6047.35 s = 1.68 h), PERSEPHONE spends a Δv of 0.29 m s^{-1}. Assuming a day as enough time from the arrival at the station keeping point until the capture of the target, it would represent a Δv of 4.19 m s^{-1}.

EDT deployment: Once the capture of the debris is achieved (Figure 5b), the spool of the tether must release the whole length of the electrodynamic tether. This separation is performed in the R-bar direction (see Figure 5c) thanks to the gravity gradient, a phenomenon in space that acts in two masses linked by a cable. As the thrown net is deployed already with 15 m of distance, the gravity gradient already generates tension. This initial deployment can be assisted with the attitude control thrusters of PERSEPHONE. The brake system masters the release velocity of the EDT, and gradually decreases it at the end of the deployment to prevent any risk of bounce, longitudinal oscillations, or rupture.

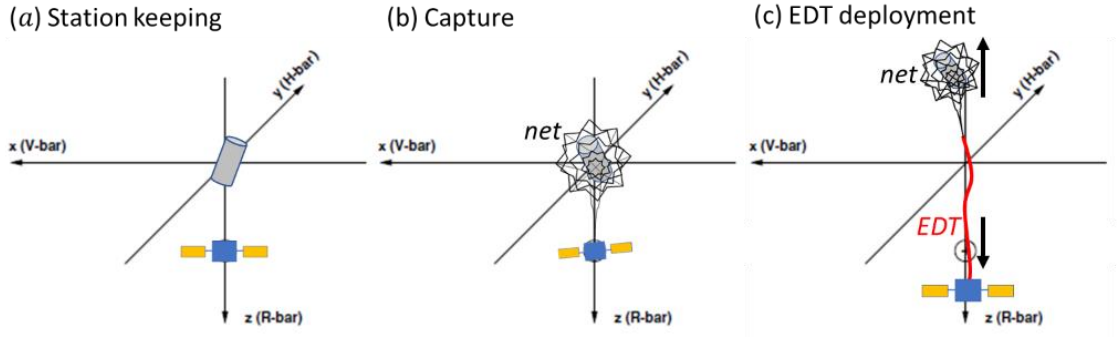

Figure 5: Net-EDT state before, during and after the target's capture.

Descent with EDT: The descent trajectory using an EDT is a spiral, the same as using low-thrust propulsion with electric engines. It was obtained from numerical simulations with GMAT software [14] that it would take 244.45 days to descend this target from its orbit down to 310 km altitude (see next phase). To do so, the propulsion module parameters were settled as if they were electric with a continuous thrust whose value changes depending on the altitude.

Impulsive maneuver for controlled atmospheric re-entry: Between 10% and 20% of the mass of large debris can survive the atmospheric re-entry [15], and just descending the debris passively to re-enter the atmosphere would result in an uncontrolled re-entry with an impacting zone difficult to predict, resulting in possible casualties. For this reason, it is necessary to make a final boost after descending with the EDT. According to Delaval [16], the SPOUA (South Pacific Ocean Uninhabited Area) is the largest unpopulated ocean space on the planet where more than 260 satellites have fallen since 1971 because of the casualty factor, it is optimal for re-entry and end-of-life disposition of satellites.

To obtain the value of a suitable altitude to perform the last boost, a trade-off was performed between the minimum Δv cost required and the lowest altitude possible just using the EDT, considering that the flight path angle at 120 km altitude must be less than -1.5° (necessary for re-entry). The results were that the spacecraft can use the EDT to descend to an orbit of 310 km altitude and then perform a boost with a Δv cost of 101.45 m s^{-1}. This strategy saves 50 % fuel compared to a standard deorbit using only chemical propulsion (see 4. Propulsion subsystem).

Overview: The whole mission has a total time duration of 347 days (maximum), without considering the launch and the re-entry time which in this case are negligible. This is a very classical duration, raising no specific problem, and coherent with the mission requirements document. The total Δv cost of the mission is 305 m s^{-1} for the less optimal scenario using a piggyback launch, and 160 m s^{-1} for a dedicated launch.

3. Electrodynamic tether

The innovative aspect for the descent phase of the target is the use of an EDT directly linked to the net. The use of this propulsive solution can save propellant mass and decrease the overall cost of the mission. Electrodynamic tethers interact with the magnetosphere. As it moves relative to the Earth magnetic field an electromotive force is generated across the tether. Following Faraday's law of induction, the motional electric field can be written as in Equation 2.

$$\vec{E}_m = \overrightarrow{v_{system}} \times \vec{B} \tag{2}$$

$\overrightarrow{v_{system}}$ represents the velocity vector of the system (EDT + plasma), $\vec{B}$ the magnetic field and $\vec{E}_m$ the motional electric field. Using the Ohm's law, the projection of the motional electric field drives a current $\vec{I}$ along the tether length cable

DOI: 10.13009/EUCASS2022-7219

L. Using the Lorentz force $\vec{F}$ the tether can induce a drag force which will decrease the progressively the altitude of the system.

$$\vec{F} = \int_0^L I\vec{dl} \wedge \vec{B} \tag{3}$$

The electrons from the plasma are collected on the tether cable which takes the role of the anode. The electron emitter is placed at the extremity of the EDT inside the spacecraft, and it is composed of an array of carbon nanotubes. This device was studied by S. Kawamoto [17].

3.1 Drag force, length, and descent phase time

Finding a good compromise between the time of descent and the tether length is important to know the intensity of the drag force that can be generated by the tether at a given altitude. Using Figure 6 as a reference [18], it is possible to obtain the information needed to compute the intensity along the cable.

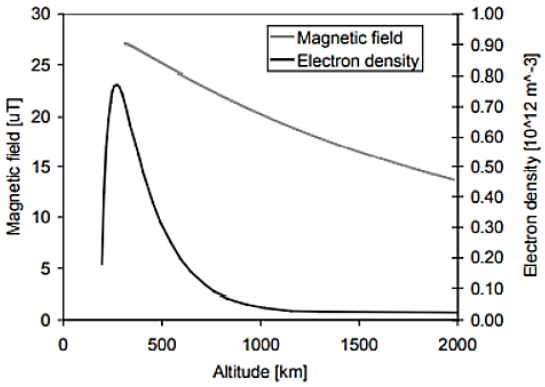

Figure 6: Magnetic field intensity and electron density in LEO [18].

Table 1: Parameters and numerical computation for the intensity, the force and the tether's length.

Altitude (km)	n_{plasma} (m^{-3})	B (T)	I_{max} (A)	F (N)
800	6.00E+10	2.30E-05	1.112	0.014
700	1.00E+11	2.40E-05	1.894	0.024
600	1.80E+11	2.50E-05	3.479	0.047
500	2.80E+11	2.60E-05	5.519	0.077
400	3.90E+11	2.70E-05	7.833	0.113
300	6.70E+11	2.75E-05	13.581	0.200
d_{eff} (m)	**m_e (kg)**	**V (V/m)**	**e (C)**	**L (m)**
0.005	9.11E-31	186000	1.60E-19	894.113

Table 1 is used to compute the force and intensity generated by the EDT. The parameters used for the study were d_{eff} which represents the effective diameter of the tether, m_e is the mass of an electron, V is the electromotive force, e is the elementary charge, and L is the tether length. The assumptions were the following: the tether is vertically oriented, the magnetic field and the velocity of the system are horizontal, so they are perpendicular and constant over the cable of the tether. Plasma density n_{plasma} is assumed to be constant over the cable length whose resistance is considered negligible. The maximal intensity I_{max} is obtained by integrating the current increment received over a small part of the tether cable. Similarly, by integrating the Lorentz force formula using the maximal intensity over the tether length it is possible to find the magnitude F of the force generated by the tether.

$$I_{max} = en_{plasma}d_{eff}\left(\frac{8evB}{9m_e}\right)^{\frac{1}{2}}L^{\frac{3}{2}} \tag{4}$$

$$F = \frac{3}{5}B^{\frac{3}{2}}en_{plasma}d_{eff}\left(\frac{8ev}{9m_e}\right)^{\frac{1}{2}}L^{\frac{5}{2}} \tag{5}$$

DOI: 10.13009/EUCASS2022-7219

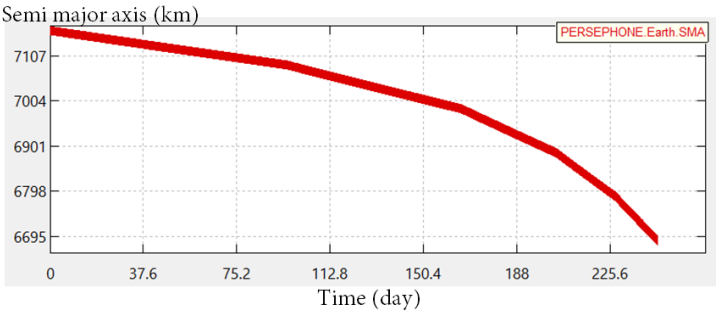

Figure 7:GMAT simulation for descent time.

Once the maximal intensity and force are computed thanks to Equations 4 and 5, several simulations using GMAT [14] were conducted to evaluate the time of the descent phase. For the trade-off of the EDT length versus the descent time, it was used the Excel solver tool. It resulted that a 894 m EDT offers a good compromise with a descent time of 244.45 days (see Figure 7).

3.2 Risk of debris collision with EDT

Another fundamental parameter considered was the risk of catastrophic failure due to a cut of the tether by other debris. To ensure that such an event does not happen, a 7-independent branches EDT (see Figure 8) resulted as the best option to decrease this risk. According to the design study, it was estimated that the tether mass is about 53 kg.

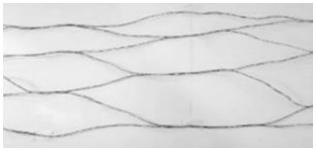

Figure 8: 7-branches EDT [19].

The probability to be cut by debris during the descent was evaluated by modelling the tether as an 894 m long plate with 2 mm thickness and 30 cm width, where the width was assumed considering the strands moving away from each other with a certain amplitude, and the thickness corresponds to the diameter of the strands. Considering that the situation is modelled assuming a Poisson law of rare events it is possible to extract the mean number of collisions per year λ that can be computed using Equation 6. F corresponds to the encountered flux of debris on a given orbit, S is the exposed surface, and ΔT is the horizon of analysis in this case equal to one year.

$$\lambda = F \cdot S \cdot \Delta T \tag{6}$$

$$\lambda = \Delta T \cdot \int_{h=0}^{tether\ length} F \cdot l \cdot dh \tag{7}$$

$$\lambda = \Delta T \cdot \Delta S \cdot \sum_{k=0}^{N} F_k \tag{8}$$

Table 2: Flux of the debris population according to the orbit and the size.

Radius (km)	Flux 1 mm (1/m²/yr)	Flux 10 mm (1/m²/yr)	Flux 10 cm (1/m²/yr)	Flux 1 m (1/m²/yr)	Flux > 1 m (1/m²/yr)
7174	3.898E-03	3.75E-05	7.918E-07	8.215E-08	1.504E-09
7173.777	3.9E-03	3.719E-05	7.969E-07	8.268E-08	1.503E-09
7173.554	3.925E-03	3.666E-05	8.028E-07	8.324E-08	1.504E-09
7173.331	3.925E-03	3.669E-05	8.06E-07	8.303E-08	1.504E-09
7173.108	3.926E-03	3.666E-05	8.081E-07	8.308E-08	1.506E-09
∑ flux tether	**0.0196**	**1.85E-04**	**4.006E-06**	**4.142E-07**	**7.521E-09**

DOI: 10.13009/EUCASS2022-7219

In the case of the study, this law is rewritten as in Equation 7 and discretized as Equation 8 with $F_{k,}$ the flux received on the specific discretization element. The chosen discretization is represented by samples of 223 m of tether cable at altitudes between 796 and 795.106 km because it is the altitude where the flux is the most concentrated. Moreover, the flux is not variating enough to take a smaller discretization. Table 2 shows the reported fluxes extracted from the ESA-MASTER database for different sizes of debris and according to the radius.

The results of the computation are stored in Table 3. Two cases were studied. The first one concern a frontal collision with the tether and debris. The second one is when the debris collides with the tether on the edge. The exposed surface ΔS was computed doing the product between the chosen discretization and the length L. Lastly, the mean number of collisions per year is given by multiplying the total flux for a dedicated debris size by the exposed surface.

Table 3: Number of collisions per year over a tether of 894m according to the debris size.

Side	L (m)	ΔS	λ 1 mm (col/yr)	λ 10 mm (col/yr)	λ 10 cm (col/yr)	λ 1 m (col/yr)	λ > 1 m (col/yr)
Frontal	0.3	66.9	1.31	1.24E-02	2.68E-04	2.77E-05	5.03E-07
On the edge	0.002	4.46E-01	8.73E-03	8.24E-05	1.79E-06	1.85E-07	3.35E-09

Based on the results, the risk is acceptable for a mission duration that last one year. The biggest threat to the mission comes from the smallest debris. Surely, at least 1 mm debris will enter the collision sphere of the tether in a year. However, this computation was done considering the worst-case scenario, for debris size between 1 mm and 10 mm the number of collisions per year is smaller because it has a good chance to pass between the strands. Moreover, even if one thread is cut the other one ensures the redundancy of the system. For bigger debris, collision avoidance is possible by modulating the electric current of the cathodes. Although the tether cable by itself is not visible from the ground, the system spacecraft + debris could probably be visible both by radar and telescope.

3.3 EDT mechanical analysis

Concerning the material of the tether, anodized aluminum has been considered the best option because of its high electrical conductivity and emissivity thanks to the anodization process. The low density of the material allows having a relatively light system. In Table 4 are reported all the characteristics of the material.

Table 4: Anodized aluminium properties.

Melting point T (°C)	Conductivity C ($S.m^{-1}$)	Emissivity ε	Density ρ (g/cm^3)	Young's modulus E (GPa)	Ultimate strength σ (MPa)
660	37.7E+06	0.77	2.7	69	310

The Stephan-Boltzmann law has been used for computing the temperature of the tether. The solar flux received per unit area M was computed in Equation 9 considering an absorption coefficient α = 1 which represents the worst-case scenario. C_0 is the solar constant which is equal to 1368 W m^{-2}. The temperature T(K) is computed in Equation 10 is 147.55 °C which is under the melting point of the material.

$$M = \alpha C_0 \tag{9}$$

$$T(K) = \left(\frac{M}{\sigma \varepsilon}\right)^{\frac{1}{4}} \tag{10}$$

To ensure that the tether will not be damaged because of the tension induced by the gravity gradient on the cable, Hao Wen [20] suggests that the tension computation can be performed assuming that the mass of the tether is negligible. For two objects orbiting at different altitudes, the equations of motion are Equations 11 and 12, where μ corresponds to the standard gravitational parameter, ω is the common orbital angular rate of PERSEPHONE and the debris, m_{sat} is the mass of the deorbiting satellite, m_{debris} is the mass of the debris, r_{sat} is the altitude of the deorbiting satellite, and r_{debris} the altitude of the debris.

$$\frac{\mu \cdot m_{sat}}{r_{sat}^2} - m_{sat}\omega^2 r_{sat} = T \tag{11}$$

$$\frac{\mu \cdot m_{debris}}{r_{debris}^2} - m_{debris}\omega^2 r_{debris} = -T \tag{12}$$

DOI: 10.13009/EUCASS2022-7219

Solving the system, the calculation of the tension is expressed by Equation 13.

$$T = \frac{\mu \cdot m_{sat} m_{debris}}{r_{sat}^2 r_{debris}^2} \frac{r_{debris}^3 - r_{sat}^3}{m_{sat} r_{sat} + m_{debris} r_{debris}} \tag{13}$$

The tension computation was studied according to two subphases of the descent: the beginning and the end. Table 5 shows the numerical result of this study. The stress generated by the tension is computed taking into consideration the computed tension and the cross-section area A of the 7-branches tether.

The computation of stress created by the last boost of the thruster was done considering a system of two masses linked by the tether with the gravity force negligible in front of the thrust generated by the engine. Considering the worst-case scenario where the angle between the thrust direction and the tether is equal to 0º, the absolute value of the tension on the tether cable is equal to the thrust generated during the last boost. As the value of the generated stress on the tether is widely under the ultimate stress value of the aluminum, the integrity of the tether is covered even during this phase of the mission.

Table 5: Tension and stress calculation results.

	μ (m^3/s^2)	m_{sat} (kg)	m_{debris} (kg)	r_{sat} (m)	r_{debris} (m)	A (m^2)	T (N)	σ (MPa)
Highest altitude	3.986005E+14	400	2575	7173106	7174000	2.2E-05	1.00	0.045
Lowest altitude	3.986005E+14	400	2575	6689106	6690000	2.2E-05	1.24	0.056
Last boost	NA	NA	NA	NA	NA	2.2E-05	556	25.3

4. Propulsion subsystem

The use of EDT for the descent phase was compared against a chemical propulsion alternative that consists of a single impulsive maneuver directly from the target's orbit aiming for a direct atmospheric re-entry (descent and re-entry all in one). It resulted in a Δv cost of 204.31 m s^{-1} for the chemical option against 101.45 m s^{-1} for EDT, which means that the implementation of the EDT implies a save of 50 % propellant. The propulsion subsystem is composed not only by this EDT (see 3. Electrodynamic tether) but also complemented by multimode chemical propulsion (see Figure 9) that serves for orbital transfer maneuvers, rendezvous operations, and the final boost that leads the group spacecraft + debris into a controlled atmospheric re-entry.

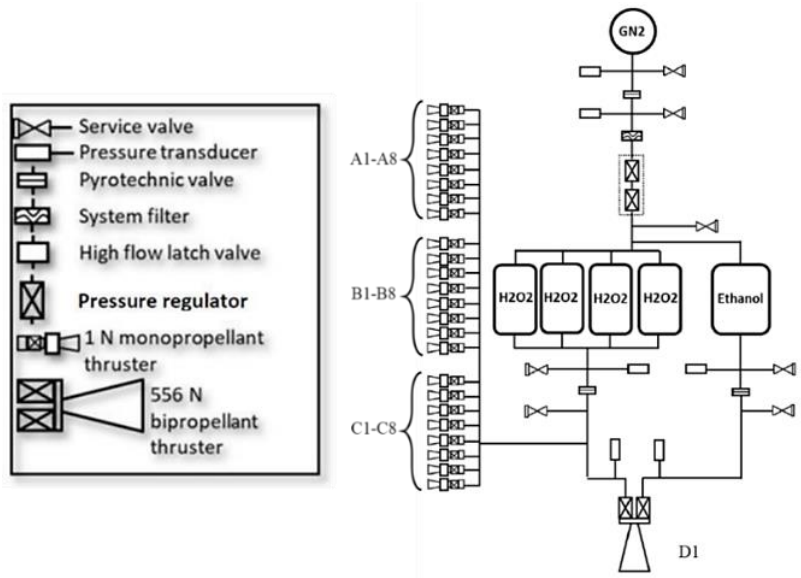

Figure 9: Simplified architecture of the multimode chemical propulsion: bipropellant with monopropellant.

4.1 Selection of the complementary propulsion type

The cold gas and plasma propulsion systems do not allow to perform a maneuver for the controlled atmospheric re-entry, because of the low thrust provided. That fact is critical in the mission and therefore they are discarded. Concerning the solid propulsion type, it is not convenient for a mission that require multiple impulses, because once it

DOI: 10.13009/EUCASS2022-7219

ignites it cannot stop. After performing some trade-offs, it resulted as suitable option a multimode propulsion that uses bipropellant for the main thruster, and monopropellant for the attitude control thrusters.

4.2 Propellant selection

Monopropellant and bi-propellant thrusters use commonly hydrazine, which is highly toxic, corrosive, and dangerous to handle and store. The non-toxicity of the propellant is a determinant factor for the selection of the propulsion subsystem, and the use of hydrazine as propellant was specifically required to avoid in the high-level mission requirements. The hydrogen peroxide (H2O2) is a green alternative, and its application for satellites is currently under development for both monopropellant and bipropellant propulsion types. It is good to note that at 95 % H202 can be explosive but adopting the right safety measures the operational risk can meet acceptable levels.

4.3 Propellant mass analysis

Mani [21] discuss the procedure to design a bipropellant propulsion system using H2O2 as oxidizer and ethanol (C2H5OH) as fuel, and it served as reference for the dimensioning of the PERSEPHONE propulsion subsystem. They suggest that the specific impulse (I_{sp}) for such thrusters is 315 s, therefore it is possible to compute the propellant mass for the whole mission, considering that the mass pre and post debris capture is relatively different. The Tsiolkovsky equation (Equation 14) was widely used to compute the propellant mass for all the different phases where thrusters ignite to perform maneuvers, where g_0 stands for the standard gravity and m_i and m_f are respectively the initial and final masses of the spacecraft during each phase.

$$\Delta v = I_{sp} g_0 \ln\left(\frac{m_i}{m_f}\right) \tag{14}$$

To be able to compute the mass propellant for all the different phases, an initial dry mass of 400 kg was proposed as it is a typical value for a mini satellite, which is the biggest category that can be launched in piggyback with a VEGA launcher [22]. Additionally, a margin of 20% additional propellant mass was included in the computations for attitude corrections, Δv losses, and collision avoidance maneuvers. By doing this, the propulsive exigences are overestimated and can be optimized afterward in an iterative process. The resultant propellant masses are shown in Equation 15 and were computed taking the total Δv estimated for the piggyback launch (see 2.3 Mission profile and analysis).

$$\begin{aligned} m_{Total} &= m_{Reach795km} + m_{Rendezvous} + m_{StationKeeping} + m_{Re-entry} \\ &= (30 + 32.3 + 4.2 + 100)kg \;=\; 166.5\,kg \end{aligned} \tag{15}$$

It is assumed a mass mixing ratio of Oxidizer/Fuel of 4.5 [21], therefore there is a mass distribution of 30.27 kg ethanol and 136.23 kg H2O2.

4.4 Main thruster

The critical parameter for the selection of the main thruster is the Δv required for the last boost maneuver that leads to a controlled atmospheric re-entry. At the altitude of such maneuver (310 km) the Δv of 101.45 m s^{-1} must be reached during a 10% of the orbital period (according to the mission requirements defined), which represents 544.33 s. With the expression $t_{burn} = (m\Delta v)/F_{thrust}$ where the mass m is 2975 kg (vehicle plus the debris in the last mission phase), it is obtained a required thrust F_{thrust} of a minimum of 556 N.

4.5 Attitude control thrusters

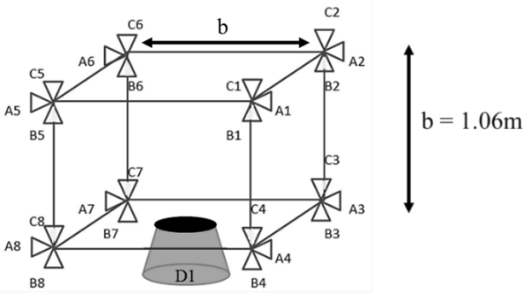

Figure 10: Attitude control thrusters' configuration.

It was defined in the system requirements that the vehicle must be agile during the capture of the debris, either with rotation or translation. For that reason and for redundancy, 24 small thrusters are used as shown in Figure 10.

DOI: 10.13009/EUCASS2022-7219

Translation: it was found that the smallest hop (see Figure 4) for the rendezvous-approach phase requires a Δv of 0.000159 m s^{-1}. Therefore, the mass m of PERSEPHONE (maximum 400 kg) multiplied by Δv gives the Minimum Impulse Bit (BIT) required, equal to 0.0636 N s. Considering that 4 attitude control thrusters together will perform every hop, then each one must have a BIT of less than 0.016 N s.

Rotation: to compute the minimum rotation speed, it was proposed the discretization of the spacecraft as a cube with a side length of 1.06 m (see Figure 10), where four attitude thrusters together would perform a rotation (i.e., A1, A4, A6, A7). The inertia is $I = (mb^2)/6 = 74.9$ kg m² and (from the BIT computed) the minimum torque produced by 4 thrusters is $T = (4 \times 0.016\ N) \times 1.06\ m = 0.067$ N m, consequently, the angular speed is $\omega = T/I = 0.05^o\ s^{-1}$, which is compliant with the system requirement of an angular rotation speed precision of less than $0.5^o\ s^{-1}$.

There is no problem to fulfill these specifications for the main and attitude control thrusters with equipment off-the-shelf. If required, some minor adaptations and additional qualifications can be made.

5. Capture subsystem

The capture subsystem is composed of several components: a net for the capture, the 7-branches EDT linked to the net, an ejection system, a speed-brake mechanism, and a spool.

A comparison of different capture methods led to the choice of a net to capture the debris. Compared to a rigid mechanism, this flexible option facilitates the complexity of capturing tumbling targets and works for both dead satellites and rocket bodies. Although this capture solution seems to be promising the capture phase will be critical. In fact, the ejection of the net from the spacecraft is definitive and it is not possible to eject the net a second time. Studies dealing with net design are a key point in the success of the mission.

5.1 Capture net

The net plays a major role in the capture of the debris and must be designed carefully to englobe the debris perfectly. For that, the use of an algorithm that computes the convex hull of the target is an option to estimate the surface of the net. The QHull algorithm [23] takes in argument several coordinates within the 3D Model of the target. The code then computes the smallest volume and surface that englobes all the coordinates' points (see Figure 11).

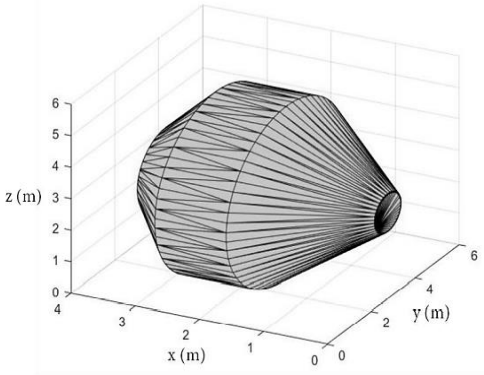

Figure 11: Convex hull of Ariane 5 upper stage.

The results computed by the algorithm indicated a convex hull area for the target of 73.6 m^2 and a convex hull volume of 51.7 m^3. The study was led on two different shapes of the net, a square, and a hexagon. Figure 12 shows the dimensions of a net for both cases.

The margins were computed considering at first a room for 0.2 % of failure for the net. This unreliability allocation is one subdivision that is included in the 1 % probability of failure of the entire mission. The net may be unproperly located and oriented after the ejection. Considering ± 1° error in angular position, ± 1 m error in positioning linked to the precision of the attitude control subsystem at 15 m of the target, the deviation is equal to $\sigma = 15 \times \tan(1°) = 0.26$ m in all directions.

Using a Gaussian distribution non-truncated with a unilateral distribution, the probability P of being under 1° corresponds to $P > 0.998$. Reading the tables of statistics, the margin Z should be minimum $Z = 2.88\ \sigma = 0.75$ m on each side of the net. The same computation should be done for a 1 m error in position. The final chosen margin for the net is 1.5 m at least. To simplify the study, the net is assumed to be made of aluminum and it is composed of 250 threads of 0.5 mm each, with a dry mass of 5.4 kg. In further studies, it is recommended to consider advanced fibers such as Dyneema or Zylon for the material.

DOI: 10.13009/EUCASS2022-7219

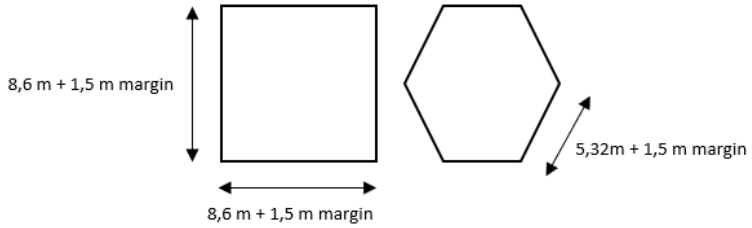

Figure 12: Dimensions for two net shape options.

5.2 Net Ejection mechanism

The deployment of the net is achieved thanks to an ejection system that was studied by Q. Gao [24]. The mechanism is composed of a storage capacity for the net (where the net is folded), net corner masses, and a cap. According to the shape of the net, the number of masses can be adapted. The ejection is carried out in two steps, the outstretching of the net and the deployment. The cap attached to the center of the net is responsible for the outstretching and helps to keep the good ejection direction. On the other hand, the corner masses are used for the deployment of the net.

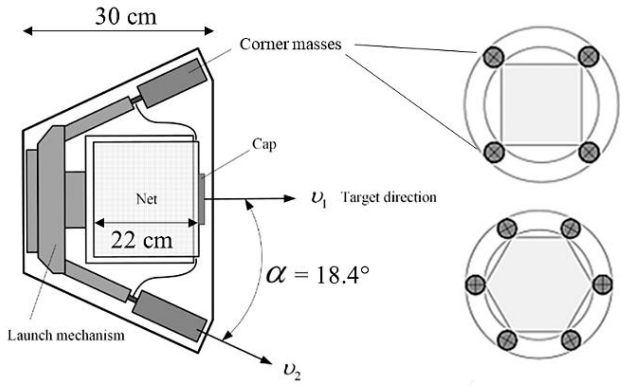

Figure 13: Ejection mechanism [24].

Figure 13 is shown how the ejection system can be adapted to the shape of the net and the number of corner masses. For PERSEPHONE mission, it was considered corner masses of 500 g each ejected with a velocity of 20 m s^{-1}. To guarantee a proper distancing between the debris and PERSEPHONE, it was computed the necessary recoil velocity of the spacecraft. This velocity also helps the deployment of the EDT, and it was estimated to be 0.14 m s^{-1} for a squared shape and 0.16 m s^{-1} for a hexagonal shape in the opposite direction of the ejection. The dimension of the net container was estimated considering the case with a squared-shape net.

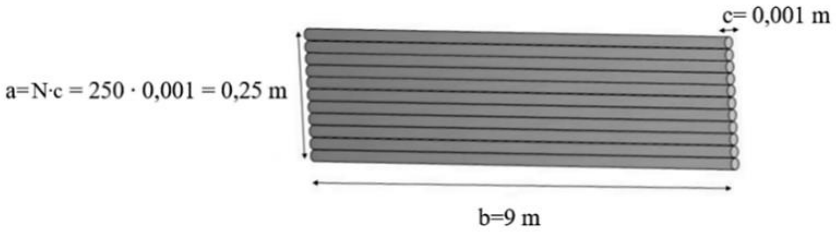

Figure 14: Threads of the squared net perfectly aligned.

To compute the volume of the net container, a perfectly aligned threads net was considered as in Figure 14. To this volume, a factor 4 is added to better cope with the real condition when the threads are not perfectly aligned. The volume of the net container considering the margin is estimated to be a cube with sides of 22 cm.

According to Misra [25], the corner masses are useful to close the net around the debris. Those masses are attached via a cinch-cord thread that goes along the net perimeter. When the debris is wrapped, the cord will be tithed because of the momentum induced by the masses getting away from PERSEPHONE spacecraft when the tether is released. The α angle in Figure 15 was estimated considering the general geometry of the ejection system (see Figure 13), representing the direction vector in which the corner masses are going to be ejected.

DOI: 10.13009/EUCASS2022-7219

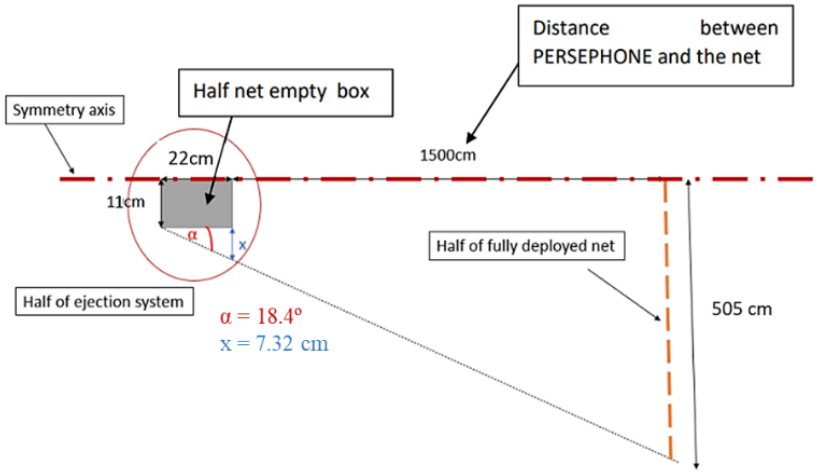

Figure 15: Geometry of the layout when the net is ejected.

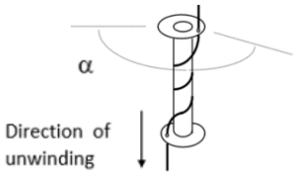

Figure 16: Brake mechanism for the EDT [26].

The tether (which is linked to the net) is coiled on a spool, and a brake mechanism comes to slow down the speed of the EDT release and prevent a stroke. The brake takes advantage of the friction of the tether wired on a cylinder (see Figure 16). Thanks to this mechanism it is possible to control the surface between the cable and the cylinder. A small step motor enables to vary the winding angle α to the desired value, hence controlling the deployment velocity of the cable. It could be possible to have two of them in case of a problem occurs on the first one.

6. Spacecraft's architecture and mass budget

To assess an initial estimation of the mass budget and dimensions, COTS (Commercial Off-The-Shelf) components were selected in agreement with the system requirements. Arranging the components of the different subsystems, it was proposed the preliminary architecture of PERSEPHONE shown in Figure 17 -left, where it is illustrated a general integration of the EDT and the net in the capture subsystem. Assembling PERSEPHONE inside the payload compartment of VEGA C as a piggyback launch would require the use of the VESPA +R carrying system [22] (see Figure 17-right), where the secondary payload goes inside VESPA +R (mini, micro, or nano spacecraft) and the main passenger goes integrated just above. One can appreciate that there is enough room for optimization and that PERSEPHONE can indeed be launched as a piggyback.

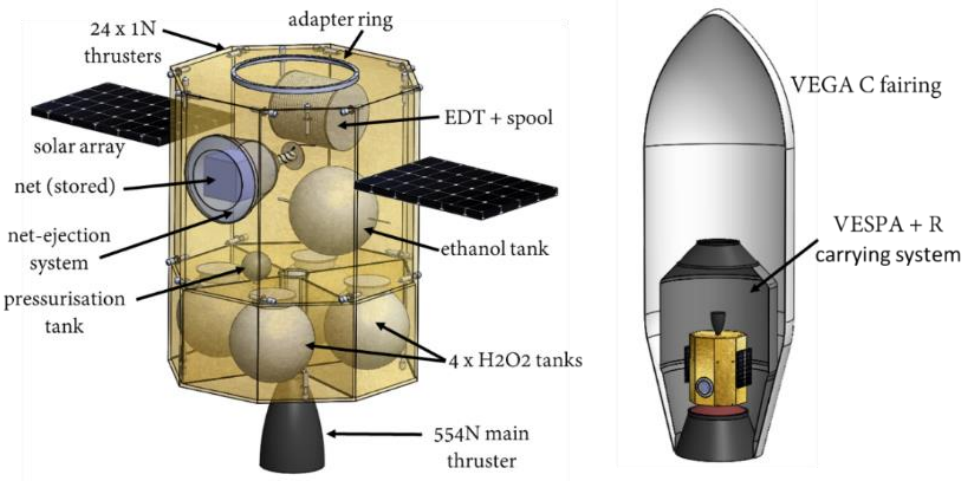

Figure 17: PERSEPHONE spacecraft (left) and its integration in VEGA C launcher as piggyback payload (right).

DOI: 10.13009/EUCASS2022-7219

Concerning the initial mass budget, PERSEPHONE has an estimated total mass of 366.3 kg including an additional margin of 20 % over the propellant mass and the overall mass of the structures. Taking that oversized total mass into consideration, the spacecraft falls into the category of minisatellite (a type of Small Sat). The mass budget distribution is presented in Figure 18, and just the propulsion and structure subsystems themselves represent 96.5 % of the whole spacecraft with a dry mass of 205 and 150 kg respectively. Therefore, it is possible to reduce the vehicle's mass and size by optimizing the mission trajectory, therefore the propulsive exigences and consequently the other subsystems and architecture iteratively.

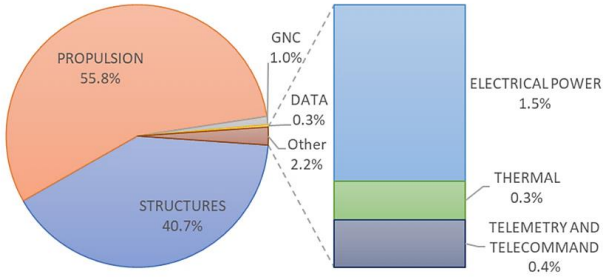

Figure 18: Mass budget distribution of the spacecraft subsystems.

Conclusion

This work is the result of a first study on the preliminary design of the PERSEPHONE mission, which has covered several aspects of an ADR mission: a deep review of the space legislation (especially about sustainability), the definition of the target and its characterization, trajectory and maneuver analysis, the design of the EDT and trade-offs to find a compromise with the time of the orbital descent phase, design of the capture subsystem, architecture definition, selection of COTS components, and many other.

The new approach to ADR mission presented in this paper proposes the use of an EDT complemented with multimode chemical propulsion to deorbit large-sized space debris from LEO, and the results show no infeasibility. The early preliminary design suggests that PERSEPHONE is a mini spacecraft of 367 kg that can deorbit a 2500 kg debris from an altitude of around 800 km, with a mission duration of less than a year. Moreover, the selected components are off-the-shelf allowing to reduce the cost, the time of development, and the complexity of the system.

After future optimization, it is expected to enhance the performance of PERSEPHONE to reach even bigger target (aiming Envisat). Further studies include the EDT dynamics, capture dynamics for non-cooperative targets, mission trajectory optimization, and detailed design of the architecture.

Acknowledgements

Special thanks and appreciation to Christophe Bonnal, space debris expert at CNES, for his strong engagement with all his valuable and rich mentoring during this project.

Sincere thanks to every international expert who gave advice in different domains:

-Dr. Satomi Kawamoto (Research Unit II, Research and Development Directorate at Japan Aerospace Exploration Agency) for her advice about the EDT and for providing her results.

-Dr. Arun Misra (Professor at McGill University in Canada and expert in tethers) for his help with the design of the EDT, the net, and the corner masses.

-Dr. Eleanora Botta (Assistant Professor in the Department of Mechanical and Aerospace Engineering, University at Buffalo, NY) for her personal guidance about the optimization of the net's size with the convex hull algorithm.

The work presented here was done together with Priyesh Rao Bangady Killur and Mathieu Couasnon.

References

[1] The European Space Agency, "Space debris by the numbers," 10 May 2022. [Online]. Available: https://www.esa.int/Safety_Security/Space_Debris/Space_debris_by_the_numbers.

[2] LeoLabs, "Quantifying Conjunction Risk in LEO," 9 January 2020. [Online]. Available: https://leolabs-space.medium.com/quantifying-conjunction-risk-in-leo-e6eee8134211.

[3] C. Bonnal and D. S. McKnight, "IAA Situation Report on Space Debris," 2016.

DOI: 10.13009/EUCASS2022-7219

[4] D. McKnight, R. Witner, F. Letizia, S. Lemmens, L. Anselmo, C. Pardini, A. Rossi, C. Kunstadter, S. Kawamoto, V. Aslanov, J. -C. Dolado Perez, V. Ruch, H. Lewis , M. Nicolls, L. Jing, S. Dan, W. Dongfang, A. Baranov and D. Grishko, "Identifying the 50 statistically-most-concerning derelict objects in LEO," *Acta Astronautica,* vol. 181, pp. 282-291, April 2021.

[5] J. O'Callaghan, "Hope for solving space debris," Aerospace America, April 2022. [Online]. Available: https://aerospaceamerica.aiaa.org/features/hope-for-solving-space-debris/.

[6] Inter-Agency Space Debris Coordination Committee, "IADC Space Debris Mitigation Guidelines," 2007.

[7] ISO International Organization for Standardization, "ISO/DIS 24113 Space systems — Space debris mitigation requirements," ISO, 2021.

[8] "Space Launch Report: Ariane 5 Data Sheet," 24 October 2021. [Online]. Available: https://www.spacelaunchreport.com/ariane5.html.

[9] D. Capdevila, "LA PRODUCTION DES LANCEURS ARIANE 5," CAPCOM ESPACE, [Online]. Available: http://www.capcomespace.net/dossiers/espace_europeen/ariane/ariane5/production_ariane5_lanceurs.htm. [Accessed 14 December 2021].

[10] Dominic Ford, "ARIANE 5 R/B," 20 November 2021. [Online]. Available: https://in-the-sky.org/spacecraft.php?id=27387.

[11] Arianespace, "Vega: User's Manual," 2014.

[12] W. Fehse, Automated Rendezvous and Docking of Spacecraft, New York: Cambridge University Press, 2003.

[13] W. Changxuan and G. Pini, "Guidance, navigation and control for autonomous R-bar proximity operations for geostationary satellites," *Journal of Aerospace Engineering,* vol. 231, no. 3, pp. 452-473, 2016.

[14] National Aeronautics and Space Administration NASA, *General Mission Analysis Tool (GMAT) [Computer software]. Version R2020a,* 2022.

[15] C. Bonnal, J. -M. Ruault and M. -C. Desjean, "Active debris removal: Recent progress and current trends," *Acta Astronautica,* p. 51–60, 2013.

[16] J. Delaval, "BASICS ABOUT CONTROLLED AND SEMI-CONTROLLED REENTRY," 16 11 2018. [Online]. Available: https://blogs.esa.int/cleanspace/2018/11/16/basics-about-controlled-and-semi-controlled-reentry/.

[17] S. Kawamoto, Y. Okawa, S. Yoshimura, S. Nishida, A. Nakajima, S. Kitamura, N. Kyoku and M. Cho, "Electrodynamic tether systems for debris removal," in *9th Spacecraft Charging Technology Conference*, Tsukuba, 2005.

[18] M. Kruijff, "Tethers in Space : A Propellantless Propulsion In-Orbit Demonstration," Delft, 2011.

[19] S. Kawamoto, Y. Ohkawa, T. Okumura, K. Iki and H. Okamoto, "Performance of Electrodynamic Tether System for Debris Deorbiting: Re-evaluation Based on the Results of KITE Experiments," in *69th International Astronautical Congress (IAC)*, Bremen, 2018.

[20] H. Wen, D. Jin and H. Hu, "Advances in dynamics and control of tethered satellite systems," *Acta Mechanica Sinica,* 2008.

[21] K. V. Mani, F. Topputo and A. Cervone, "Chemical Propulsion System Design for a 16U Interplanetary CubeSat," in *69th International Astronautical Congress*, Bremen, 2018.

[22] Arianespace, "Small Spacecraft Mission Service Vega-C user's manual," Arianespace, 2020.

[23] E. M. B. Charles M. Barenes, "A quality index for net-based capture of space debris," *Acta Astronautica,* 2020.

[24] Q. Gao, Q. Zhang, Z. Feng and Q. Tang, "Study on launch scheme of space-net capturing system," *PLOS ONE,* 2017.

[25] I. Sharf, B. Thomsen, E. Botta and A. Misra, "Experiments and simulation of a net closing mechanism for tethered-net capture of space debris," *Acta Astronautica,* 2017.

[26] "Les Tethers, end-of-studies project," 1999.